Geol. Mag. **152** (*6*), *2015, pp. 1073–1084. © Cambridge University Press 2015*
doi:10.1017/S0016756815000217

Late Permian mafic rocks identified within the Doba basin of southern Chad and their relationship to the boundary of the Saharan Metacraton

J. GREGORY SHELLNUTT*†, TUNG-YI LEE*, CHIH-CHENG YANG‡, SHIN-TAI HU‡, JONG-CHANG WU‡, KUO-LUNG WANG§ & CHING-HUA LO¶

*National Taiwan Normal University, Department of Earth Science, 88 Tingzhou Road Section 4, Taipei 116, Taiwan
‡Chinese Petroleum Corporation-Taiwan, Exploration and Development Research Institute, Wen Fa Road, Miaoli 36042, Taiwan
§Academia Sinica Institute of Earth Sciences, 128 Academia Road Section 2, Taipei 115, Taiwan
¶National Taiwan University, Department of Geosciences, P.O. Box 13–318, Taipei 106, Taiwan

(*Received* 5 January 2015; *accepted* 17 March 2015; *first published online* 6 May 2015)

Abstract – The Doba gabbro was collected from an exploration well through the Cretaceous Doba basin of southern Chad. The gabbro is composed mostly of plagioclase, clinopyroxene and Fe–Ti oxide minerals and displays cumulus mineral textures. Whole-rock ^{40}Ar–^{39}Ar step-heating geochronology yielded a Late Permian plateau age of 257 ± 1 Ma. The major and trace elemental geochemistry shows that the gabbro is tholeiitic in composition and has trace element ratios (i.e. $La/Yb_N > 7$; $Sm/Yb_{PM} > 3.4$; $Nb/Y > 1$; $Zr/Y > 5$) indicative of a basaltic melt derived from a garnet-bearing mantle source. The moderately enriched Sr–Nd isotopes (i.e. $I_{Sr} = 0.70495$ to 0.70839; $\varepsilon Nd_{(T)} = -1.0$ to −1.3) fall within the mantle array (i.e. OIB-like) and are similar to other Late Permian plutonic rocks of North-Central Africa (i.e. $I_{Sr} = 0.7040$ to 0.7070). The enriched isotopic composition of the Doba gabbro contrasts with the more depleted compositions of the spatially associated Neoproterozoic post-Pan-African within-plate granites. The contrasting Nd isotope composition between the older within-plate granites and the younger Doba gabbro indicates that different mantle sources produced the rocks and thus may mark the southern boundary of the Saharan Metacraton.

Keywords: Late Permian, Saharan Metacraton, ^{40}Ar–^{39}Ar dating, Doba basin, Chad.

1. Introduction

North-Central Africa was a relatively stable cratonic (i.e. Saharan Metacraton) platform after the Late Proterozoic to Early Palaeozoic Pan-Africa Orogeny (Kroner, 1980; Rogers, Unrug & Sultan, 1995; Abdelsalam, Liegeois & Stern, 2002; Dostal *et al.* 2002; Caby, 2003; Caby & Monie, 2003; Veevers, 2003; Toteu, Penaye & Djomani, 2004; Bailey & Woolley, 2005; Abdelsalam, Gao & Liegeois, 2011; Liegeois *et al.* 2013). The Early Palaeozoic to Late Palaeozoic was a period dominated by the deposition of marine and terrestrial sediments with sporadic influence of regional collision and extensional tectonics (Fabre, 1988; Guiraud *et al.* 2005). However, during Late Carboniferous to Early Permian time, the period of relative regional geological quiescence in North-Central Africa ended as the Variscan orogeny began and led to the formation of fold belts in the west (e.g. Morocco) and the development of major regional faulting to the east and south (Genik, 1993; Guiraud *et al.* 2005).

By Late Permian time, the first of five magmatic episodes began (Liegeois *et al.* 1983; Rahaman *et al.* 1984; Weis, Liegeois & Black, 1987; Almond, 1991; Wilson & Guiraud, 1992; Wilson *et al.* 1998; Bailey & Woolley, 2005). Late Permian to Early Triassic magmatic rocks of North-Central Africa are reported from Morocco to Egypt and include anorogenic alkaline igneous complexes from central Libya (Sirt), Mali (Tadhak), Niger (Damagaram, Matsena) and Sudan (Nuba Mountains, Kordofan). The igneous complexes, although spatially unrelated, may be related to regional extensional environments associated with mantle upwelling as some of the intrusions have isotope composition consistent with their being derived from a source with a 'Dupal' type mantle signature (Liegeois *et al.* 1983; Rahaman *et al.* 1984; Weis, Liegeois & Black, 1987; Hohndorf, Meinhold & Vail, 1994; Wilson *et al.* 1998; Burke, 2001). If the Late Permian rocks of North-Central Africa are directly or indirectly related then the precise nature, duration, volumetric and areal extent is more speculative than definitive owing to the limited amount of geochronological and geochemical data.

Chad is situated within the Saharan Metacraton between the major geological boundaries of the Pan-African Orogeny, that is, the Central African Orogenic Belt (CAOB) (i.e. Oubanguides Orogen) in the south, the Trans-Saharan Orogen in the west and the Arabian Nubian Shield in the east (Abdelsalam, Liegeois &

†Author for correspondence: jgshelln@ntnu.edu.tw

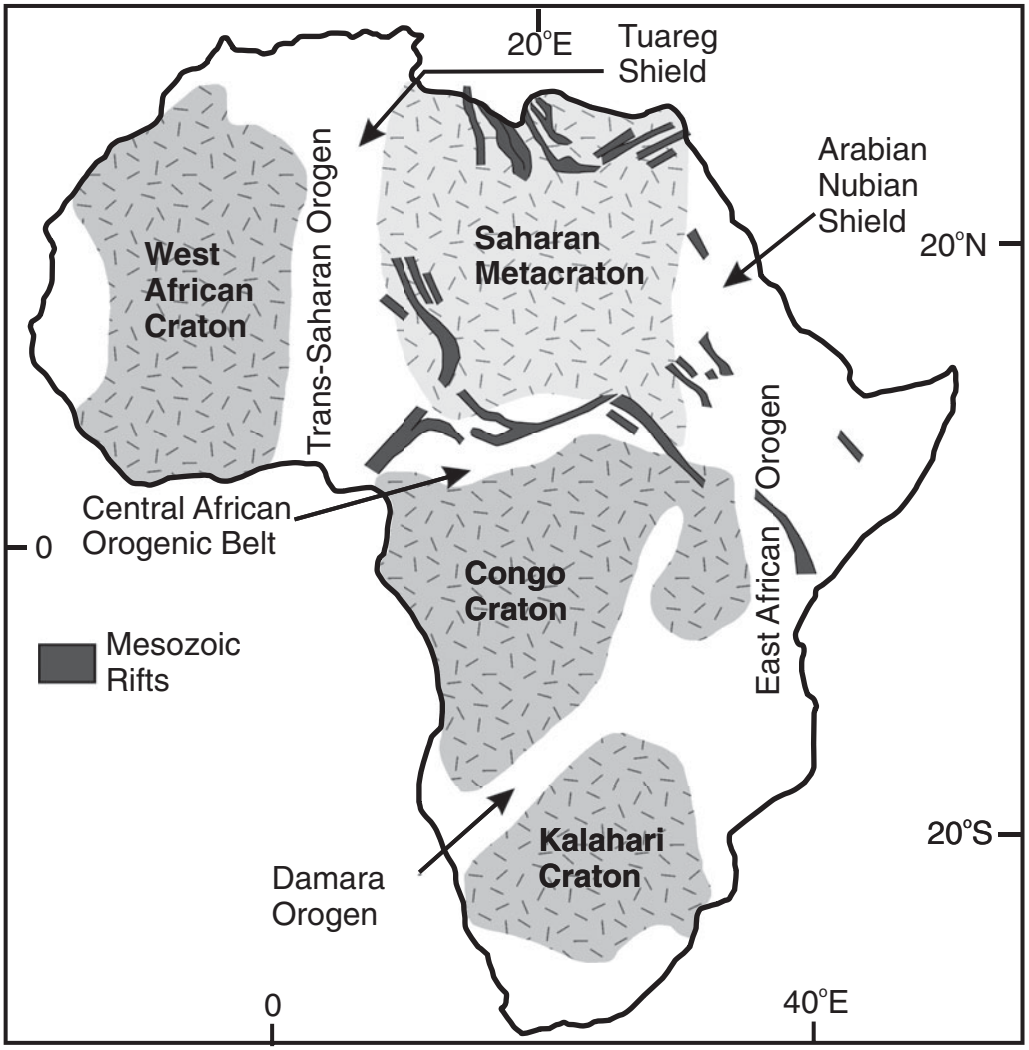

Figure 1. Distribution of Precambrian cratons, metacratons and orogenic belts of Africa (modified from Abdelsalam, Gao & Liegeois, 2011).

Stern, 2002; Liegeois *et al.* 2013) (Fig. 1). The Saharan Metacraton should contain rocks associated with one or more of the five magmatic stages outlined by Wilson *et al.* (1998). However, compared to many regions of North-Central Africa, Chad is relatively understudied, partially because the Sahara desert, which transitions into Sahal, covers a large portion of the country. Owing to petroleum exploration, the basement geology is partially known from exploration well analysis and seismic profiling in some regions. The discovery of undeformed gabbroic rocks within an exploration well from the Cretaceous–Palaeogene Doba basin near the boundary between the Saharan Metacraton and the CAOB in southern Chad provides an opportunity to constrain the petrogenesis of post-Pan-African magmatism in a region where it has not been previously documented.

This study presents the results of whole-rock ^{40}Ar–^{39}Ar step-heating analyses, whole-rock major and trace elemental data and whole-rock Sr–Nd isotopes of a gabbro obtained from the basement of the Doba basin of southern Chad. The data are used to determine the petrogenetic history of the gabbro and evaluate if it is associated with any of the regional tectonomagmatic stages previously identified in North-Central Africa.

2. Geological background

Chad is located in North-Central Africa and is composed of Precambrian rocks covered by Phanerozoic volcanic and sedimentary rocks. The Precambrian rocks are found in the Tibesti Mountains north of N'Djamena, the Ouddai Massif at the eastern border and central areas of Chad, the Guera Massif in the centre and the Yade and Mayo Kebbi massifs in the south (Fig. 2a). The Tibesti, Ouddai and Guerra massifs and other pre-Neoproterozoic blocks of North-Central Africa form the Saharan Metacraton, which is an amalgamation of structurally related, contemporaneous Archaean to Proterozoic rocks which were heavily remobilized during the Late Proterozoic Pan-African Orogeny (Abdelsalam, Liegeois & Stern, 2002; Liegeois *et al.* 2013). The boundaries of the Saharan Metacraton are delineated by the Trans-Saharan Orogen (i.e. the Raghane Shear zone) in the west, the northern

https://doi.org/10.1017/S0016756815000217 Published online by Cambridge University Press

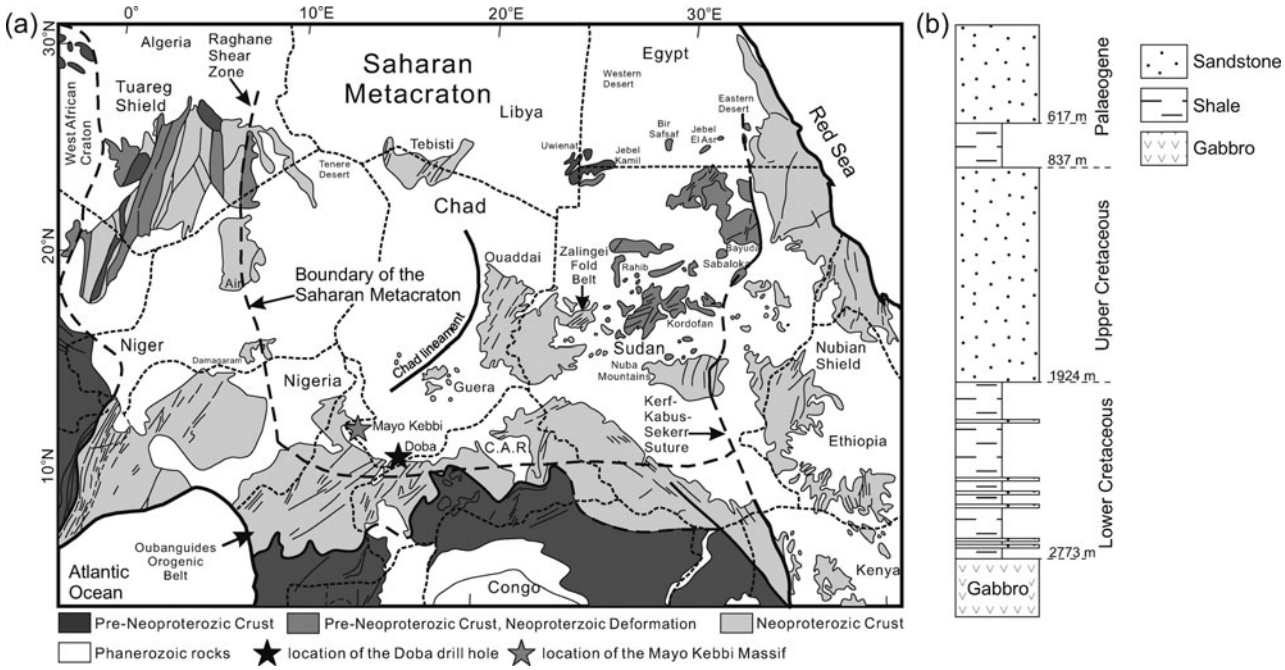

Figure 2. (a) Simplified regional geological framework map of North-Central Africa showing the boundary of the Saharan Metacraton (modified from Abdelsalam, Liegeois & Stern, 2002). Location of the Doba basin drill hole and Mayo Kebbi Massif shown as stars. (b) Stratigraphy of the drill hole within the Doba basin.

margin of the CAOB (i.e. Oubanguides Orogen) identified as the Aswa Shear Zone in the south and the Keraf–Kabus–Sekerr suture in the east (Fig. 2a). The northern boundary is located in southern Egypt and Libya and is covered by Phanerozoic sediments (Abdelsalam, Liegeois & Stern, 2002; Abdelsalam, Gao & Liegeois, 2011). In the southwest corner of Chad is the Mayo Kebbi Massif, which consists of juvenile Neoproterozoic crust that formed during and after the Pan-African Orogeny (Toteu, Penaye & Djomani, 2004; Toteu *et al.* 2006; Penaye *et al.* 2006; Isseini *et al.* 2012). The last known period of magmatism that occurred in the Mayo Kebbi Massif was the emplacement of the post-Pan-African Zabili A-type granite at ~570 Ma (Isseini *et al.* 2012). The southern parts of Chad are mostly covered by continental sediments which were deposited during Late Cretaceous to Palaeogene time. The Chad Formation is the dominant Neogene unit and comprises lacustrine sediments of the Chad Basin (Schluter, 2008).

The samples collected for this study came from an exploration well into the Doba basin of southern Chad (Fig. 2a, b). Cretaceous to Palaeogene rift basins developed in Niger, Chad and the Central African Republic as a consequence of stretching and subsidence during the break-up of Gondwana (Genik, 1993). The Doba basin is separated from the Doseo basin to the east by the Borogop strike-slip fault, which is one of many faults related to the NE–SW-trending CAOB system (Fig. 3). The Bongor basin to the north is separated from the Doba–Doseo basin by a basement high. Nearly all Cretaceous to Palaeogene basins in southern and western Chad have significant petroleum reserves (Genik, 1993). The gabbro was discovered near the bottom of the ~3000 m deep bore hole (Fig. 2b). Overlying the gabbro is ~2800 m of thick layers of Palaeogene sandstones and shales to Lower Cretaceous, variably thick sandstones and shales. The uppermost gabbro was collected at 2800 m and samples were obtained at 50 m intervals. The sample numbers of the gabbro (i.e. 2800, 2850, 2900, 2950, 3000, 3050) correspond to the depth of collection from the exploration well.

3. Petrography

The Doba gabbro is medium to coarse grained and has an intergranular cumulus texture. The major crystals are plagioclase (~50 vol. %), clinopyroxene (~35–40 vol. %), magnetite (~2–3 vol. %) and ilmenite (~2–3 vol. %) with accessory orthopyroxene (< 5 vol. %), apatite (≤ 1 vol. %), quartz (≤ 1 vol. %) and pyrite (<< 1 vol. %). The plagioclase crystals comprise ~50 vol. % of the rock and are typically tabular and 1–2 cm in length. Some are altered to saussurite or sericite but overall most are fresh. Clinopyroxene crystals are euhedral to subhedral with tabular to angular shapes. They are typically ≈1 cm in length with some altering to chlorite with aggregates of titanite and Fe–Ti oxide minerals. In some cases the clinopyroxene shows textures indicative of post-plagioclase crystallization but in general it appears that both the clinopyroxene and plagioclase crystallized at the same time. Euhedral to anhedral ilmenite and Ti-rich magnetite are observed within or along grain boundaries of the clinopyroxene. The oxide minerals are typically < 1 cm long. Euhedral, tabular orthopyroxene crystals were observed and are most commonly found together with

https://doi.org/10.1017/S0016756815000217 Published online by Cambridge University Press

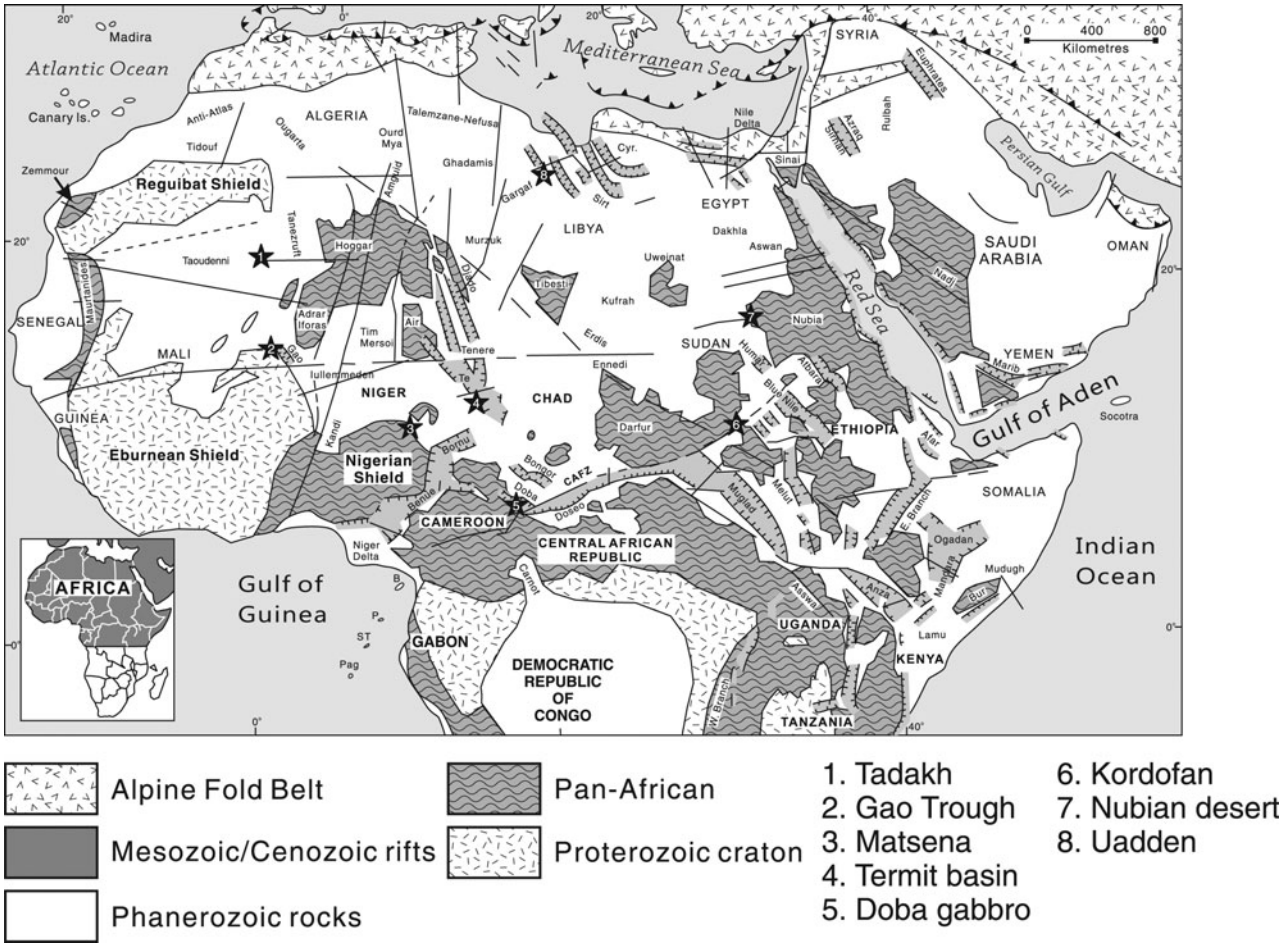

Figure 3. Regional-scale structural map of North Africa showing the locations of rift basins and Late Permian magmatic rocks (modified from Guiraud *et al.* 2005). 1 – Tadakh (262 ± 7 Ma); 2 – Gao Trough (260 ± 13 Ma and 275 ± 14 Ma); 3 – Matsena (258 ± 5 Ma); 4 – Termit basin (266 Ma); 5 – Doba gabbro (257 ± 1 Ma); 6 – North Kordofan (268 ± 6.5 Ma and 270 ± 3.5 Ma); 7 – Nubian desert (250 ± 5.2 Ma, 257 ± 8 Ma and 265 ± 12 Ma); 8 – Uaddan (256 Ma).

the clinopyroxene and Fe–Ti oxides. Euhedral apatite occurs in all samples and is spatially associated with clinopyroxene or interstitial to plagioclase. Quartz was observed in only a few samples where it was associated with apatite and interstitial to plagioclase.

4. Methods

4.a. ^{40}Ar–^{39}Ar geochronology

Whole-rock chips were crushed and sieved to 20–40 mesh (850–425 μm), ultrasonically cleaned in distilled water, dried and handpicked under a microscope to remove grains with visible impurities. Samples and standards were irradiated at the McMaster Reactor, Canada. Irradiation neutron flux was monitored using the LP6 Biotite standard (Odin *et al.* 1982) with an ^{40}Ar–^{39}Ar age of 128.5 ± 0.5 Ma, relative to the 28.305 ± 0.036 Ma Fish Canyon Sanidine monitor standard (Renne *et al.* 2010). After irradiation, the standard and samples were degassed using a double-vacuum resistance furnace in steps from 600 to 1500 °C with a 30-min heating schedule. Furnace temperatures were calibrated to ±2 °C. Argon isotopes were measured using a VG1200 mass spectrometer at National Taiwan University. Isotopic results were corrected for mass discrimination, interfering nuclear reactions, procedural blanks and atmospheric argon contamination. Plateau ages are defined for the dates and errors calculated from the sum total gas comprising three or more continuous heating steps and corresponding to at least 50 % of the total ^{39}Ar released, and the individual fraction ages overlap at the 2σ confidence level (Fleck, Sutter & Elliot, 1977). The results can be found in Table S1 in the online Supplementary Material available at http://journals.cambridge.org/geo.

4.b. Wavelength dispersive X-ray fluorescence spectrometry (WD-XRFS)

The samples were cut into small pieces using a diamond-bonded steel saw and were then crushed in a steel jaw crusher. The crusher was extensively cleaned after each sample with de-ionized water. The crushed samples were pulverized in an agate mill to ~200 mesh, heated to temperatures of ~110 °C and ~900 °C, respectively to determine unbound H_2O and loss on ignition (LOI). Lithium metaborate was added to the oxidized samples and fused to produce a glass disc using

https://doi.org/10.1017/S0016756815000217 Published online by Cambridge University Press

Table 1. Major and trace elemental data of the Doba gabbro

Sample	2800	2850	2900	2950	3050	AGV-2 m.v. (3)	AGV-2 r.v.	BCR-2 m.v. (2)	BCR-2 r.v.	BHVO-2 m.v. (2)	BHVO-2 r.v.	BIR-1 m.v. (39)	BIR-1 r.v.	DNC-1 m.v. (2)	DNC-1 r.v.	SDC-1 m.v. (30)	SDC-1 r.v.
SiO_2 (wt%)	50.26	53.24	51.56	53.74	53.06							47.75	47.96			65.73	65.85
TiO_2	3.79	2.64	2.83	2.11	2.12							0.96	0.96			0.99	1.01
Al_2O_3	14.05	16.32	15.50	15.67	15.27							15.42	15.50			15.89	15.75
Fe_2O_3t	11.35	9.81	10.48	8.80	9.69							11.13	11.30			6.76	6.90
MnO	0.16	0.12	0.14	0.12	0.13							0.17	0.18			0.11	0.11
MgO	3.79	3.17	4.22	3.89	4.57							9.59	9.70			1.64	1.69
CaO	7.85	8.18	9.15	8.55	8.77							13.22	13.30			1.43	1.40
Na_2O	4.68	3.92	3.50	3.67	3.56							1.73	1.82			2.04	2.05
K_2O	1.35	1.10	1.12	1.27	1.20							0.03	0.03			3.22	3.28
P_2O_5	0.61	0.13	0.14	0.14	0.25							0.18	0.21			0.14	0.16
LOI	2.30	1.89	1.98	2.02	1.47												
Total	100.19	100.52	100.59	99.98	100.09												
Mg no.	39.8	39.1	44.4	46.7	48.3												
Sc (ppm)	22	18	23	19		12	13	34	33	32	32			31	31		
V	227	252	246	191		119	120	418	416	313	317			154	148		
Cr	47	41	91	81		21	17	21	18	281	280			284	270		
Co	50	23	31	22		15	16	37	37	44	45			56	57		
Ni	25	22	31	28		17	19	12	13	113	119			250	247		
Cu	69	48	49	42		53	53	25	19	128	127			103	100		
Zn	117	95	100	81		81	86	132	127	105	103			60	70		
Ga	19.3	23.0	22.0	21.0		21.0	20.0	23.3	23.0	22.0	21.7			14.2			
Rb	22.0	14.0	16.0	15.0		66.0	68.6	49.0	48.0	9.0	9.8			4.0			
Sr	816	580	513	495		654	658	354	346	395	389			147	144		
Y	23	14	15	14		20	20	37	37	26	26			18	18		
Zr	127	161	107	94		230	230	192	188	170	172			38	38		
Nb	29.9	19.8	17.9	15.7		13.8	15.0	12.6	12.5	18.0	18.0			1.5			
Cs	0.3	0.3	0.5	0.5		1.1	1.16	1.1	1.1	0.1	0.1			0.2			
Ba	1515	836	663	1222		1126	1140	697	683	148	130			118	118		
La	18.4	10.5	10.7	10.7		33.0	38.0	25.2	25.0	14.9	15.0			3.6	3.6		
Ce	39.3	21.6	22.4	21.9		67.0	68.0	53.8	53.0	37.3	38.0			9.0			
Pr	5.07	2.66	2.84	2.69		7.90	8.30	7.00	6.80	5.30	5.29			1.1			
Nd	22.5	12.0	12.9	12.2		30.2	30.0	29.7	28.0	24.7	25.0			5.0	5.2		
Sm	5.80	3.20	3.50	3.30		5.50	5.70	6.80	6.70	6.20	6.20			1.40			
Eu	1.96	1.70	1.59	1.56		1.57	1.54	2.03	2.00	2.04	2.07			0.58	0.59		
Gd	5.96	3.29	3.66	3.33		4.43	4.69	6.95	6.80	6.20	6.30			2.11			
Tb	0.87	0.52	0.56	0.52		0.62	0.64	1.07	1.07	0.92	0.90			0.38			
Dy	4.80	2.85	3.14	2.87		3.41	3.6	6.50	6.41	5.27	5.31			2.74			
Ho	0.88	0.52	0.56	0.52		0.68	0.71	1.36	1.33	1.01	1.04			0.65			
Er	2.06	1.30	1.41	1.31		1.78	1.79	3.70	3.66	2.50	2.54			1.91			
Tm	0.27	0.17	0.18	0.17		0.25	0.26	0.54	0.54	0.34	0.34			0.30			
Yb	1.53	1.04	1.11	1.04		1.62	1.60	3.49	3.50	2.01	2.00			1.98	2.00		
Lu	0.21	0.13	0.15	0.13		0.25	0.25	0.54	0.51	0.28	0.28			0.30			
Hf	3.11	3.63	2.53	2.29		4.96	5.08	4.81	4.80	4.25	4.10			0.96			
Ta	2.11	1.18	1.07	0.94		0.88	0.89	0.83	0.81	1.21	1.40			0.09			
Th	1.60	1.50	1.70	1.50		6.20	6.10	6.10	6.20	1.20	1.29			0.30			
U	0.40	0.30	0.20	0.20		1.90	1.88	1.70	1.69	0.40	0.42			0.10			
La/Yb_N	8.6	7.2	6.9	7.4													
Eu/Eu*	1.02	1.59	1.35	1.42													

Mg no. – $(Mg^{2+}/(Mg^{2+}+Fe2^{2+}))*100$; N – normalized to chondrite values of Sun & McDonough (1989); m.v. – measured value; r.v. – recommended value.

a Claisse M4 fluxer. The major oxide concentrations were determined by WD-XRFS using a PANalytical Axios mAX spectrometer at National Taiwan Normal University in Taipei. The long-term precision for SDC-1 standard reference material on 30 analyses is better than ± 0.5 % on all elements except MgO, Na_2O and P_2O_5, which are better than ± 2 % (Table 1). The long-term precision for BIR-1 standard reference material on 39 analyses is better that ± 0.5 % on all elements except Na_2O and K_2O, which are ± 2 % (Table 1).

4.c. Inductively coupled plasma mass spectrometry (ICP-MS)

Trace elements were analysed using an Agilent 7500cx inductively coupled plasma mass spectrometer (ICP-MS) at National Taiwan University, Taipei, Taiwan. Approximately 20 mg of powder from each sample was digested in a Teflon beaker using a combination of HF, HNO_3 and HCl. Initially, samples were heated in closed beakers with HF and HNO_3 for at least two days and then dried. Two millilitres of 6N HCl was added to each sample and then left to dry. This step was repeated. An additional 2 ml of 1N HCl was added to each sample and then centrifuged. The supernatant was extracted from each beaker into a new one. If there was solid residue left in the beakers then the procedure was repeated until all samples were fully digested. Samples were diluted using 2 % HNO_3 and a Rh and Bi spike was added for the internal standard. The standard reference materials run with samples are AGV-2 (andesite), BCR-2 (basalt), BIR-1 (basalt) and DNC-1 (dolerite). The

https://doi.org/10.1017/S0016756815000217 Published online by Cambridge University Press

Table 2. Whole-rock Sr and Nd isotope data of the Doba gabbro

Sample	Rb (ppm)	Sr (ppm)	$^{87}Rb/^{86}Sr$	$^{87}Sr/^{86}Sr$	$\pm2\sigma_m$	I_{Sr}	Sm (ppm)	Nd (ppm)	$^{147}Sm/^{144}Nd$	$^{143}Nd/^{144}Nd$	$\pm2\sigma_m$	$\varepsilon Nd_{(0)}$	$\varepsilon Nd_{(T)}$	f (Sm/Nd)	$T_{DM}-1$
2800	22	816	0.078	0.708679	10	0.70839	5.75	22.5	0.1545	0.512513	5	−2.4	−1.1	−0.21	1636
2950	15	496	0.089	0.705368	10	0.70504	3.3	12	0.1663	0.512522	5	−2.3	−1.3	−0.15	2010
2900	16	513	0.090	0.705283	11	0.70495	3.5	13	0.1628	0.512513	6	−2.4	−1.3	−0.17	1900
2850	14	580	0.070	0.705662	8	0.70541	3.2	13	0.1488	0.512505	8	−2.6	−1.0	−0.24	1512

Rb, Sr, Sm and Nd concentrations were obtained by ICP-MS and precisions better than ± 2 %. The results of isotopic measurements for Sr and Nd reference materials are NBS-987 (Sr) = 0.710248 ± 3 (2σm). JMC (Nd) = 0.511813 ± 10 (2σm). f(Sm/Nd) is defined as $((^{147}Sm/^{144}Nd)/0.1967-1)$. $\varepsilon Nd_{(T)}$ is calculated using an approximate equation of $\varepsilon Nd_{(T)} = \varepsilon Nd_{(0)} - Q*f*T$; in which Q = 25.1 Ga^{-1}, f = f(Sm/Nd), Tage = 0.257 Ga. $T_{DM}-1 = (1/\lambda)*\ln(1+((^{143}Nd/^{144}Nd)_m-0.51315)/((^{147}Sm/^{144}Nd)_m-0.2137))$; $\lambda = 0.00654\ Ga^{-1}$.

precision for all trace elements is better than ± 5 % relative. The results can be found in Table 1.

4.d. Thermal ionization mass spectrometry (TIMS)

Approximately 75–100 mg of whole-rock powder was dissolved using a mixture of HF-$HClO_4$ in a Teflon beaker at ~100 °C. The procedure was repeated in some cases to ensure total dissolution of the sample. Strontium and rare earth elements (REEs) were separated using polyethylene columns with a 5 ml resin bed of AG 50W-X8, 200–400 mesh. Neodymium was separated from other REEs using polyethylene columns with a Ln resin as a cation exchange medium. Strontium was loaded on a single Ta-filament with H_3PO_4, and Nd was loaded with H_3PO_4 on a Re-double-filament. $^{143}Nd/^{144}Nd$ ratios were normalized to $^{146}Nd/^{144}Nd$ = 0.7219 and $^{87}Sr/^{86}Sr$ ratios to $^{86}Sr/^{88}Sr$ = 0.1194. The Sr isotope ratios were measured using a Finnigan MAT-262 thermal ionization mass spectrometer (TIMS) whereas the Nd isotopic ratios were measured using a Finnigan Triton TIMS in the Mass Spectrometry Laboratory, Institute of Earth Sciences, Academia Sinica, Taipei. The $2\sigma_m$ values for all samples are less than or equal to 0.000011 for $^{87}Sr/^{86}Sr$ and less than or equal to 0.000008 for $^{143}Nd/^{144}Nd$. The measured isotope ratio during analysis of the JMC Nd standard is 0.511813 ± 0.000010 ($2\sigma_m$) and for NBS987-Sr is 0.710248 ± 0.00001 ($2\sigma_m$). The results can be found in Table 2.

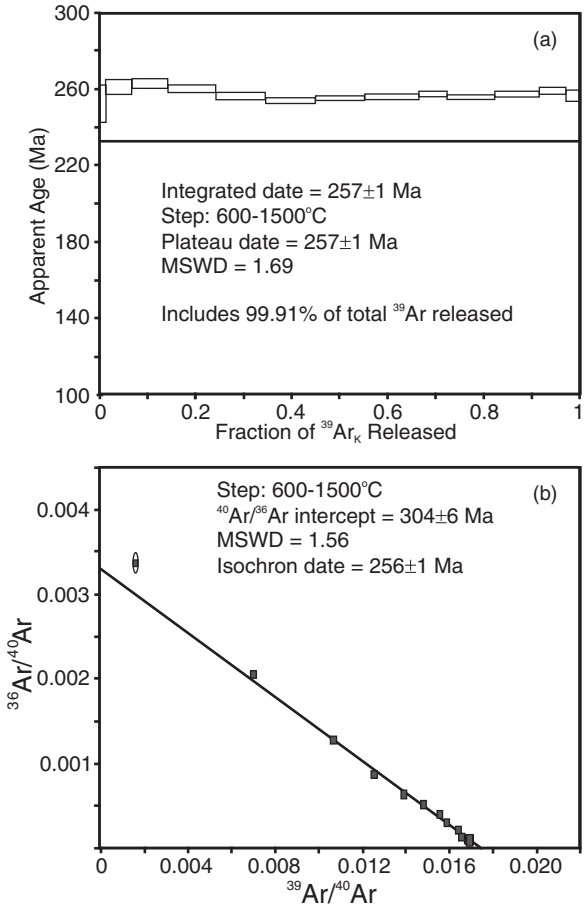

Figure 4. (a) Age spectra of the step-heating analysis for the Doba gabbro (sample 3000). (b) $^{36}Ar/^{40}Ar$–$^{39}Ar/^{40}Ar$ isotope correlation diagram.

5. Results

5.a. Geochronology

Sample number 3000 was selected for whole-rock ^{40}Ar–^{39}Ar step-heating analyses. It was located at the 3000 m mark of the drill hole in the Doba basin, which places the sample ~200 m below the unconformable contact with the overlying Lower Cretaceous sediments and solidly within the gabbro away from possible weathered surfaces. The result yielded a plateau age of 257 ± 1 Ma (Fig. 4a). In the $^{36}Ar/^{40}Ar$ versus $^{39}Ar/^{40}Ar$ correlation diagrams, the data produce a linear array with a mean square of the weighted deviates (MSWD) equal to 1.56. Furthermore, the isochron age (256 ± 1 Ma) is within error of the plateau age (Fig. 4b).

5.b. Whole-rock geochemistry

The rocks from the Doba gabbro are transitional to subalkaline with slightly more intermediate compositions (e.g. SiO_2 = 50.3 to 53.7 wt %). The rocks have relatively low Mg no. values (Mg no. = $(Mg^{2+}/(Mg^{2+}+Fe^{2+}_{total}))*100$) between 39 and 48, which is consistent with magma evolution and low MgO wt % (i.e. MgO = 3.2 to 4.6 wt %) relative to Fe_2O_3t wt % (i.e. Fe_2O_3t = 8.8 to 11.4 wt %). Sample 2800 is a little different from the others as it has the highest TiO_2 (i.e. 3.8 wt %), Fe_2O_3t (i.e. 11.4 wt %), Na_2O (i.e. 4.7 wt %), K_2O (i.e. 1.3 wt %) and P_2O_5 (i.e. 0.6 wt %) and lowest SiO_2 (i.e. 50.3 wt %), Al_2O_3

https://doi.org/10.1017/S0016756815000217 Published online by Cambridge University Press

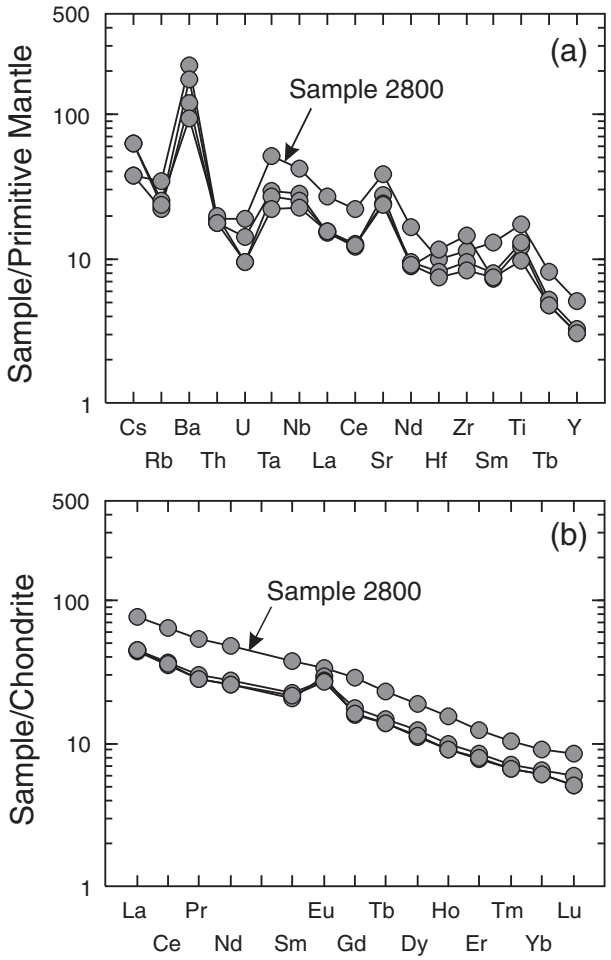

Figure 5. (a) Primitive-mantle-normalized incompatible element diagram of the Doba gabbro. (b) Chondrite-normalized rare earth element diagram of the Doba gabbro. Normalizing values are from Sun & McDonough (1989).

(i.e. 14.1 wt %) and CaO (i.e. 7.9 wt %). The remaining samples are compositionally similar to each other. The LOI is moderate with values between 1.5 wt % and 2.3 wt %.

The bulk trace element content of the rocks is very similar, although sample 2800 shows some differences relative to the other samples. The transition metals (i.e. Sc = 18–23 ppm, V = 191–252 ppm, Cr = 41–91 ppm, Co = 22–50 ppm, Ni = 22–31 ppm, Cu = 42–69 ppm) and high-field-strength elements (i.e. Zr = 94–161 ppm, Nb = 16–30 ppm, Hf = 2.3–3.1 ppm, Ta = 0.9–2.1 ppm, Th = 1.5–1.7 ppm, U = 0.2–0.4 ppm) do not show significant variation between the samples. Sample 2800 has much higher Sr (820 ppm) and Ba (1520 ppm) in comparison to the other samples (i.e. Sr = 500 to 580 ppm, Ba = 660 to 1220 ppm).

The primitive-mantle-normalized incompatible trace element patterns show that all rocks have distinct positive anomalies of Ba, Sr and to a lesser extent Ti with negative anomalies of U, La and Ce. Sample 2800 is more enriched in most incompatible elements than the other samples but their patterns are similar (Fig. 5a). The chondrite-normalized REE patterns show overall enrichment in the light REEs (La/Yb_N = 6.9 to 8.6) with positive Eu anomalies (i.e. Eu/Eu∗ = 1.3 to 1.6) within samples 2850, 2900 and 2950, whereas sample 2800 has a relatively smooth pattern similar to ocean-island basalt and has an Eu/Eu∗ value of ∼1.0 (Fig. 5b).

5.c. Sr–Nd isotope geochemistry

The initial $^{87}Sr/^{86}Sr$ values, calculated using the $^{40}Ar/^{39}Ar$ age, range from 0.70839 to 0.70495 with samples 2850, 2900, 2950 having similar values (i.e. I_{Sr} = 0.70495 to 0.70541) and sample 2800 showing the highest value (i.e. I_{Sr} = 0.70839). The Nd isotope data are relatively more uniform than the Sr isotope data with the initial $^{143}Nd/^{144}Nd$ ratios ranging from 0.51224 to 0.51225, which correspond to $\varepsilon Nd_{(T)}$ values of −1.0 to −1.3 using a CHUR value of 0.512639. The fractionation factor (i.e. f(Sm/Nd)) ratios of the gabbro range from −0.15 to −0.24 with corresponding T_{DM} ages ranging from 1512 Ma to 2010 Ma.

6. Discussion

6.a. Regional correlation of the Late Permian rocks in Northern Africa

Wilson *et al.* (1998) outlined five periods of magmatism within the African–Arabian margin of Tethys beginning from Late Permian to latest Triassic time (i.e. 256 Ma to 208 Ma) and continuing through four other stages including: Early Jurassic to Mid Jurassic (i.e. 208 Ma to 157 Ma), Late Jurassic to earliest Aptian (i.e. 157 Ma to 120 Ma), mid Aptian to mid Eocene (i.e. 119 Ma to 42 Ma) and late Eocene to recent (i.e. < 42 Ma). The Late Permian (i.e. 257 ± 1 Ma) age of the Doba gabbro is contemporaneous with the older end of Stage I magmatism. Late Permian magmatic rocks occur throughout North-Central Africa and include: the Tadhak (262 ± 7 Ma) alkaline ring complex (Mali), the Matsena (258 ± 5 Ma) alkaline granite (Nigeria), the Sirt (256 Ma) biotite-hornblende granites (Libya), Gao Trough (260 ± 13 Ma and 275 ± 14 Ma) dolerite dykes (Mali), North Kordofan (268 ± 6.5 Ma and 270 ± 3.5 Ma) anorogenic complexes (Sudan), and the Nubian desert (250 ± 5.2 Ma, 257 ± 8 Ma and 265 ± 12 Ma) igneous complexes (Sudan) (Fig. 3) (Lay & Reichelt, 1971; Liegeois *et al.* 1983; Massa & Delort, 1984; Rahaman *et al.* 1984; Weis, Liegeois & Black, 1987; Almond, 1991; Liegeois, Sauvage & Black, 1991; Hohndorf, Meinhold & Vail, 1994; Wilson *et al.* 1998). Furthermore, Genik (1993) reported a 266 Ma age of hornfels schist from the Iaguil well of the Termit basin (Niger) and attributed its deformation to thermal events related to the Variscan (Hercynian) orogeny.

Permian magmatism in North-Central Africa is attributed to rifting but the nature (i.e. passive or active) of the rifting is not clear (Wilson *et al.* 1998). The Sahara Metacraton was located near the centre of Pangaea during Permian time and there is no evidence for regional-scale plate boundary processes (i.e. plate separation or

https://doi.org/10.1017/S0016756815000217 Published online by Cambridge University Press

subduction) occurring at that time. Therefore, it is likely that localized post-Variscan orogeny tensional regimes were the major influence on the development of rift basins in the region. In many cases the magmatic rocks are geologically associated with major Pan-African tectonic lineaments that crisscross North-Central Africa (Guiraud, Issawi & Bellion, 1985; Guiraud *et al*. 2000). The parental magmas likely exploited regional structural lineaments, such as the Central African Shear Zone, Tibesti Lineament and Guinean–Nubian lineament, to reach mid to upper crustal levels and created a series of temporally associated, possibly source-related intrusions that follow regional structural trends rather than one concerted rift basin (Black & Liegeois, 1993; Wilson *et al.* 1998; Guiraud *et al.* 2000).

The Sr isotopic composition of the Doba gabbro (i.e. I_{Sr} = 0.7049 to 0.7084) is similar to other Late Permian alkaline complexes (i.e. I_{Sr} = 0.7040 to 0.7070) and suggests that there may have been a common mantle source with 'Dupal' anomaly characteristics beneath North-Central Africa during this time (Liegeois *et al.* 1983; Rahaman *et al.* 1984; Weis, Liegeois & Black, 1987; Almond, 1991; Hohndorf, Meinhold & Vail, 1994; Wilson *et al.* 1998). However, the magmatic rocks are not spatially contiguous and a large, flood basalt province has not been identified. Whether or not the individual igneous complexes are related to the same source is difficult to assess because there is limited isotopic data available for comparison. The range of I_{Sr} values is somewhat restricted (i.e. I_{Sr} = 0. 7040 to 0.7070) and indicates that a mantle component was involved in the genesis of some silicic intrusions, presumably because they were derived from mafic parental magmas, but it is also possible that crustal contamination occurred within some of the intrusions.

6.b. Petrogenesis of the Doba gabbro

The Doba gabbro is the first Late Permian mafic intrusion reported from the Doba basin of southern Chad and confirms that there was magmatism occurring in the region during a time when much of North-Central Africa was a stable craton (Rahaman *et al.* 1984; Weis, Liegeois & Black, 1987; Fabre, 1988; Vail, 1989; Almond, 1991; Guiraud *et al.* 2005). Petrographically the gabbro shows cumulus textures suggesting that it represents a relict magma chamber and/or magma conduit. The primitive-mantle-normalized incompatible element plots show distinct enrichments in Ba, Sr and to a lesser extent Ti with depletion of La, Ce and U consistent with the gabbros having accumulated plagioclase and Fe–Ti oxide minerals, and lost a residual liquid (Fig. 5) (c.f. Shellnutt *et al.* 2011). Furthermore, the rocks have Eu/Eu∗ values > 1, which is characteristic of plagioclase accumulation.

The one sample that stands out is 2800, the shallowest collected, which displays a smooth chondrite-normalized pattern without a Eu anomaly. The sample is unlikely to represent the original liquid composition because it is not fine grained (i.e. not the chilled

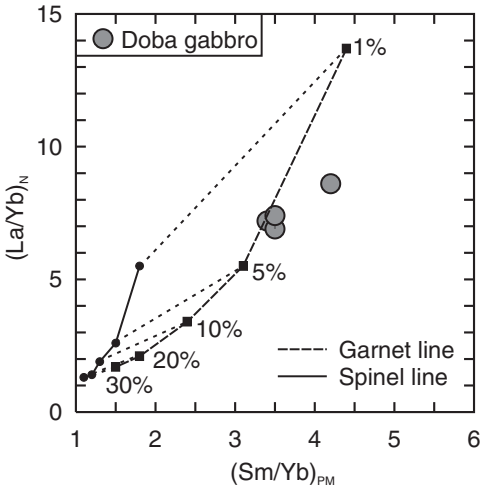

Figure 6. La/Yb_N v. Sm/Yb_{PM} of the Doba gabbros showing the partial melt line of a 5 % spinel-bearing peridotite and 5 % garnet-bearing peridotite assuming a primitive mantle composition (Sun & McDonough, 1989). Ratios normalized to chondrite (N) and primitive mantle (PM) values of Sun & McDonough (1989).

margin) and is enriched in all incompatible elements (i.e. is more likely evolved rather than primitive) but it could represent a gradual contact with another batch of magma that was injected into the chamber. Characterizing the original melt composition of the Doba gabbro is problematic owing to its cumulate nature but some trace element ratios, in particular incompatible element ratios (e.g. Th/Nb, Nb/U, REE ratios, Nb/Y), are not affected by fractional crystallization because their elements are partitioned into late-stage accessory minerals (e.g. zircon, titanite) preserving original magmatic ratios (Condie, 1997, Condie (2003; Fitton *et al.* 1997; Baksi, 2001; Campbell, 2002). Moreover, some trace element ratios can provide constraints on the likely source characteristics (i.e. depth, subcontinental lithospheric mantle (SCLM) v. sub-lithospheric mantle) of the rock as well as classification and possible tectonic setting (Condie, 1997, 2003; Fitton *et al.* 1997; Peate, 1997; Baksi, 2001; Hawkesworth & Schersten, 2007).

The emplacement of the Doba gabbro was undoubtedly within-plate owing to the regional geological setting of North-Central Africa within Pangaea at that time (Guiraud *et al.* 2005). Moreover, the high-field-strength-element-based (i.e. La–Y–Nb) tectonomagmatic discrimination diagram (not shown) of Cabanis & Lecolle (1989) shows the gabbros have a within-plate affinity. The source characteristics of the Doba gabbro are inferred from trace element ratios (i.e. La/Yb, Sm/Yb, Nb/Y, Zr/Y) and Sr–Nd isotopes. The relatively high La/Yb_N (i.e. > 7), Sm/Yb_{PM} (i.e. > 3.4), Nb/Y (i.e. > 1) and Zr/Y (i.e. > 5) ratios are likely indicative of the effects of residual garnet in the source rock and thus the parental magma originated from a garnet-bearing peridotite which implies a mantle source depth of ≥ 50 km (Fig. 6). Evidence for significant (> 5 %) crustal contamination is not obvious as the Nb/U

https://doi.org/10.1017/S0016756815000217 Published online by Cambridge University Press

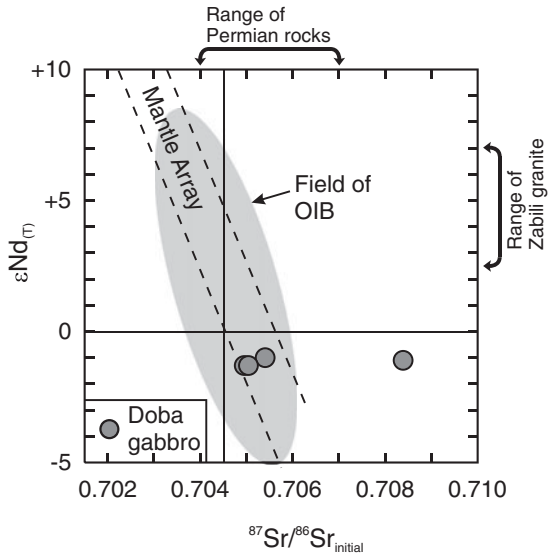

Figure 7. $\varepsilon Nd_{(T)}$ versus I_{Sr} isotope plot of the Doba gabbroic rocks showing the range of Permian rocks from North-Central Africa and the Zabili granites (data from Liegeois *et al.* 1983; Rahaman *et al.* 1984; Weis, Liegeois & Black, 1987; Hohndorf, Meinhold & Vail, 1994; Isseini *et al.* 2012). OIB – ocean-island basalt.

(i.e. > 65), Th/Nb_{PM} (i.e. < 1) and Th/Ta (< 2) ratios of the gabbro are very different from the middle to upper crust (i.e. Nb/U = < 10, Th/Nb_{PM} > 7.5, Th/Ta = > 10) and do not show chemical trends towards crustal values. Additionally, the lack of negative Ta–Nb anomalies in the primitive-mantle-normalized incompatible element patterns suggests that a crustal source was not a major contributor to the genesis of the parental magma. Similar interpretations are made for the other igneous complexes of North-Central Africa (Rahaman *et al.* 1984; Weis, Liegeois & Black, 1987; Liegeois, Sauvage & Black, 1991). The Sr–Nd isotope compositions of the gabbros show they are moderately enriched and fall along the mantle array and within the range of ocean-island basalt, although sample 2800 has a different I_{Sr} ratio (Fig. 7). The relatively enriched isotope compositions probably reflect original mantle source compositions because evidence for crustal assimilation is absent. For example, the whole-rock Nb/U values are > 65 and Th/Nb_{PM} values are < 1.0. Therefore, the parental magma of the Doba gabbro was likely basaltic, tholeiitic and derived from a garnet-bearing peridotite source.

6.c. Tectonic implications for boundary of the Saharan Metacraton

The Doba gabbro is located near or within the southern boundary of the Saharan Metacraton at the junction with the CAOB and the Trans-Saharan Orogen and is possibly the first evidence of rift-related magmatism in this region since the Pan-African Orogeny. Located ~300 km to the northwest of the Doba gabbro is the Late Neoproterozoic (i.e. 570 Ma), post-collisional Zabili A-type granitic pluton (Fig. 2a). The Zabili granite was emplaced into terranes (i.e. island arcs plus continental fragments) associated with either the Eastern Nigerian basement or the Congo Craton after the final suturing of the Saharan Metacraton and is amongst the last intrusions to be emplaced prior to Permian time (Bailey & Woolley, 2005; Isseini *et al.* 2012). Comparing the petrogenetic histories of the Zabili granite and Doba gabbro may be able to provide some constraints on the possible magma source evolution and compositions, in particular the isotopic composition, or mantle contribution in each rock type. Any difference in the isotopic compositions of the rocks could reflect important information on the region or nature of the lithosphere that melted to produce their magmas. Moreover, there are potential implications for the boundary between the Saharan Metacraton and the Congo Craton because, at the moment, it is uncertain precisely which craton the rocks have intruded. According to Abdelsalam, Gao & Liegeois (2011), the resolution of geophysical surveys (i.e. shear wave velocity data) cannot readily distinguish the southern boundary between the Saharan Metacraton and the Congo Craton.

The Zabili granite is considered to be derived by partial melting of mafic lower crust that was extracted from a juvenile mantle wedge source between 570 Ma and 600 Ma. The Nd isotopes of the Zabili granites have $\varepsilon Nd_{(T)}$ values between +2.6 and +7.0, which are indicative of a juvenile, depleted to moderately depleted source and have T_{DM} ages of 600 Ma to 1000 Ma (Fig. 7). In comparison the Doba gabbro has more enriched $\varepsilon Nd_{(T)}$ values (i.e. $\varepsilon Nd_{(T)}$ = −1.3 to −1.0) and T_{DM} ages of 1500 Ma to 2000 Ma. The mid to early Proterozoic T_{DM} values of the Doba gabbro indicate that the mantle source was significantly older than the age of magmatism whereas the Zabili granite has values which are significantly younger and close to the age of emplacement. The differences between the Nd isotopic compositions and T_{DM} values of the Zabili granites and the Doba gabbro imply they are derived from isotopically distinct mantle sources.

Abdelsalam, Gao & Liegeois (2011) suggested that the lithospheric mantle beneath the Saharan Metacraton was partially delaminated during the Pan-Africa Orogeny and thus the lithosphere is thinner than that of the surrounding cratons. The delamination of the mantle could explain the relatively depleted Nd isotopic signature of the Zabili granite as a more juvenile depleted mantle would have replaced the older lithospheric mantle. In other words, the Zabili A-type granite was derived from magmatic rocks related to the newly formed juvenile mantle after delamination whereas the Doba gabbro was derived from an older, enriched mantle source. It is possible that the Doba gabbro was derived from either a portion of the Saharan Metacraton that did not undergo partial mantle delamination, or it is a part of the Congo Craton, or CAOB. Rocks from the CAOB (i.e. Oubanguides) have T_{DM} ages between 1000 Ma and 2000 Ma, which are similar to the Doba gabbro (Abdelsalam, Liegeois & Stern, 2002). Consequently, there are at least three

https://doi.org/10.1017/S0016756815000217 Published online by Cambridge University Press

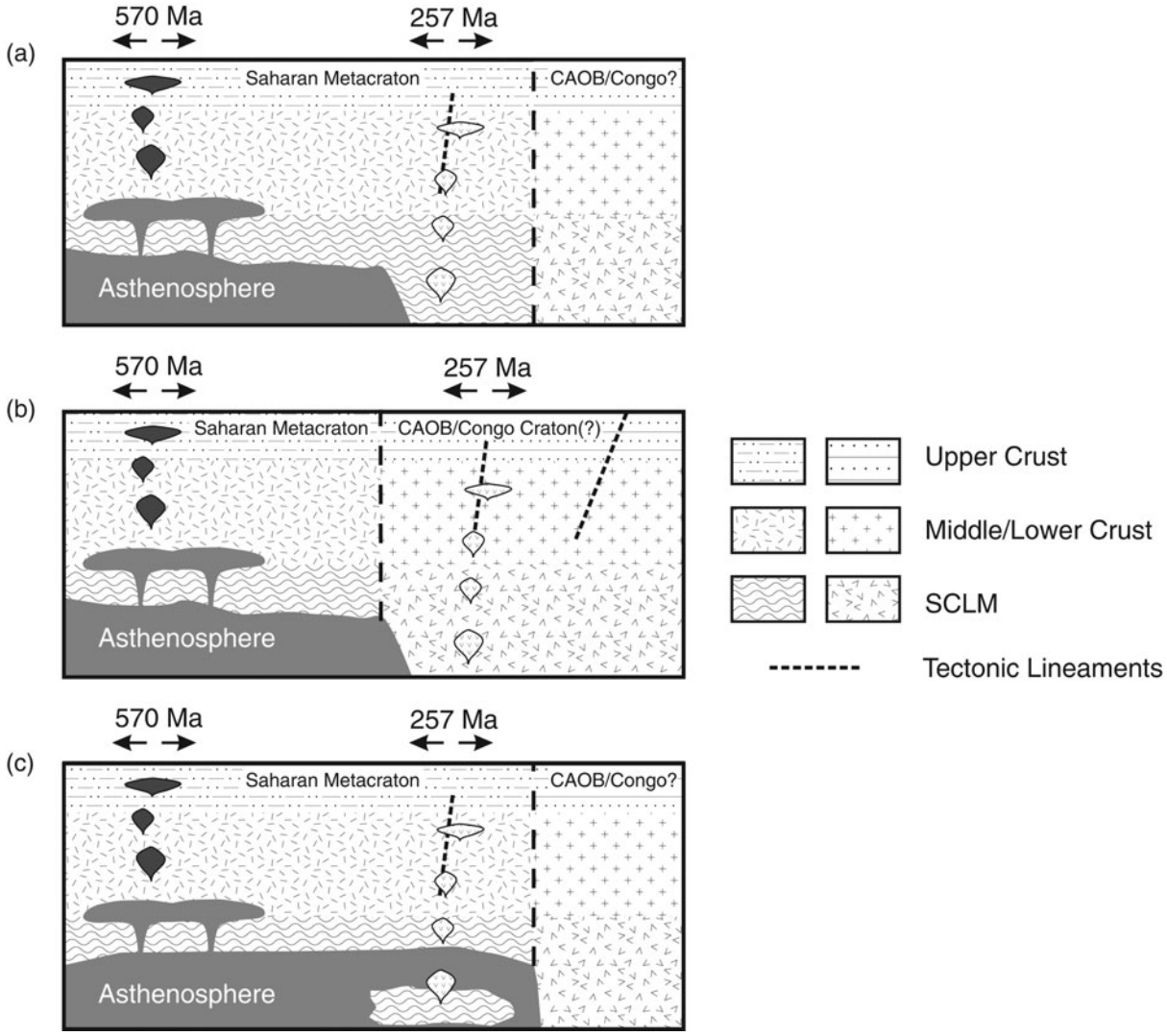

Figure 8. Three possible petrogenetic and tectonic models for the formation of the Doba gabbro: (a) the Doba gabbro was derived from the Saharan Metacraton; (b) the Doba gabbro was derived from a neighbouring craton or terranes within the Central African Orogenic Belts (CAOB); (c) the Doba gabbro was derived by melting of delaminated subcontinental lithospheric mantle (SCLM) of the Saharan Metacraton. The 570 Ma Zabili granites (570 Ma) are derived by partial melting of mafic lower crustal rocks that were derived from a depleted-mantle source. The Doba gabbro (257 Ma) was derived from a deep-mantle source. See text for details.

possible scenarios that could explain the Nd isotope variability between the Doba gabbro and the Zabili granite: (1) the Doba gabbro was derived from a portion of the Saharan Metacraton which preserved its lithospheric mantle (Fig. 8a); (2) it is a part of another craton or terrane (e.g. Congo, CAOB) and is close to the southern boundary of the Saharan Metacraton (Fig. 8b); or (3) the Doba gabbro was derived from the delaminated SCLM which sank into the asthenosphere and then melted (Fig. 8c). The third scenario is viable but less likely because the melts derived from the foundered SCLM would likely mix with more depleted, asthenospheric melts and produce a moderately depleted isotopic signature. The first two scenarios are more likely and have implications for the location of the boundary between the Saharan Metacraton and the Congo Craton. If the Doba gabbro and Zabili granite are derived from the same mantle source then they should have similar isotopic compositions because there is limited, if any, evidence for substantial (i.e. $> 5\,\%$) crustal assimilation in both intrusions, but the fact that they are very different would tend to suggest that they are derived from different terranes.

The reason for Late Permian melting is still uncertain but could be related to edge-driven convection in the mantle owing to the discrepancy in lithospheric thickness between the Saharan Metacraton and the surrounding cratons, delayed melting associated with Pan-African mantle delamination, or rifting and decompressional melting (King & Anderson, 1995, 1998; King, 2005; Elkins-Tanton, 2005). The fact that the Doba gabbro is one of the first Late Permian rocks identified in southern Chad implies that magmatism was probably volumetrically minor and not widespread. However, the true extent of Late Permian magmatism is unknown and the volume of magma is not constrained. We suggest the most likely explanation for the occurrence of Late Permian magmatism in the region is owing to rifting and partial melting of a garnet peridotite that was derived from an enriched lithospheric mantle source. The

https://doi.org/10.1017/S0016756815000217 Published online by Cambridge University Press

isotopic compositional difference between the Zabili granite and Doba gabbro may be related to the fact that they are on opposite sides of an unseen terrane boundary.

7. Conclusions

The age of the Doba gabbro is correlative with other Late Permian within-plate alkaline igneous complexes throughout North-Central Africa and testifies to regional magmatism during this time. The parental magma of the Doba gabbro was likely tholeiitic and similar to within-plate basalt. The trace element chemistry and Sr–Nd isotopes suggest the parental magma originated from an enriched garnet-bearing mantle source. We suggest that mafic melts percolated via major tectonic lineaments and reached mid to upper crustal depths. The relatively enriched Nd isotopic composition of the Doba gabbro, in comparison with the spatially associated, older, more depleted Zabili within-plate granites suggests they are derived from different mantle sources, which may indicate the presence of a terrane boundary possibly between the Saharan Metacraton and the CAOB.

Acknowledgements. We thank the constructive reviews by John Greenough and an anonymous reviewer. We also thank Phil Leat for editorial handling and Kevin Burke, J.-P. Liegeois and Chris Harris for their comments on an earlier draft of this manuscript. CPC-Taiwan is acknowledged for providing the samples for this study. This manuscript was supported by NSC project 102-2628-M-003-001-MY4 to JGS.

Supplementary material

To view supplementary material for this article, please visit http://dx.doi.org/10.1017/S0016756815000217.

References

ABDELSALAM, M., GAO, S. S. & LIEGEOIS, J.-P. 2011. Upper mantle structure of the Saharan Metacraton. *Journal of African Earth Sciences* **60**, 328–36.

ABDELSALAM, M., LIEGEOIS, J.-P. & STERN, R. J. 2002. The Saharan Metacraton. *Journal of African Earth Sciences* **34**, 119–36.

ALMOND, D. C. 1991. Anorogenic magmatism in northeast Africa. In *Geology of Libya* (ed. M. J. Salem), pp. 2495–510. Amsterdam: Elsevier.

BAILEY, D. K. & WOOLLEY, A. R. 2005. Repeated, synchronous magmatism within Africa: timing, magnetic reversals, and global tectonics. In *Plates, Plumes, and Paradigms* (eds G. R. Foulger, J. H. Natland, D. C. Presnall & D. L. Anderson), pp. 365–77. Geological Society of America, Special Paper no. 388.

BAKSI, A. K. 2001. Search for a deep-mantle component in mafic lavas using a Nb-Y-Zr plot. *Canadian Journal of Earth Sciences* **38**, 813–24.

BLACK, R. & LIEGEOIS, J.-P. 1993. Cratons, mobile belts, alkaline rocks and continental lithospheric mantle: the Pan-African testimony. *Journal of the Geological Society, London* **150**, 89–98.

BURKE, K. 2001. Origin of the Cameroon Line of volcano-capped swells. *Journal of Geology* **109**, 349–62.

CABANIS, B. & LECOLLE, M. 1989. Le diagramme La/10-Y/15-Nb/8: un outil pour la discrimination des series volcanique et la mise en evidence des processus de mélange et/ou de contamination crustale. *Comptes Redus l'Academie des Sciences* **309**, 2023–9.

CABY, R. 2003. Terrane assembly and geodynamic evolution of central-western Hogger: a synthesis. *Journal of African Earth Sciences* **37**, 133–59.

CABY, R. & MONIE, P. 2003. Neoproterozoic subductions and differential exhumation of western Hogger (southwest Algeria): new structural, petrological and geochronological evidence. *Journal of African Earth Sciences* **37**, 269–93.

CAMPBELL, I. H. 2002. Implications of Nb/U, Th/U and Sm/Nd in plume magmas for the relationship between continental and oceanic crust formation and the development of the depleted mantle. *Geochimica et Cosmochimica Acta* **66**, 1651–61.

CONDIE, K. C. 2003. Incompatible element ratios in oceanic basalts and komatiites: tracking deep mantle sources and continental growth rates with time. *Geochemistry, Geophysics, Geosystems* **4**, doi: 10.1029/2002/GC000333.

CONDIE, K. C. 1997. Source of Proterozoic mafic dyke swarms: constraints from Th/Ta and La/Yb ratios. *Precambrian Research* **81**, 3–14.

DOSTAL, J., CABY, R., KEPPIE, J. D. & MAZA, M. 2002. Neoproterozoic magmatism in southwestern Algeria (Sebkha el Melah inlier): a northern extension of the Trans-Saharan orogeny. *Journal of African Earth Sciences* **35**, 213–25.

ELKINS-TANTON, L. T. 2005. Continental magmatism caused by lithospheric delamination. In *Plates, Plumes, and Paradigms* (eds G. R. Foulger, J. H. Natland, D. C. Presnall, & D. L. Anderson), pp. 449–61. Geological Society of America, Special Paper no. 388.

FABRE, J. 1988. Les series paleozoiques d'Afrique: une approche. *Journal of African Earth Sciences* **7**, 1–40.

FITTON, J. G., SAUNDERS, A. D., NORRY, M. J., HARDARSON, B. S. & TAYLOR, R. N. 1997. Thermal and chemical structure of the Iceland plume. *Earth and Planetary Science Letters* **153**, 197–208.

FLECK, R. J., SUTTER, J. F. & ELLIOT, D. H. 1977. Interpretation of discordant $^{40}Ar/^{39}Ar$ age-spectra of Mesozoic tholeiites from Antarctica. *Geochimica et Cosmochimica Acta* **41**, 15–32.

GENIK, G. J. 1993. Petroleum geology of Cretaceous-Tertiary rift basins in Niger, Chad, and Central African Republic. *American Association of Petroleum Geology B* **77**, 1405–34.

GUIRAUD, R., BOSWORTH, W., THIERRY, J. & DELPLANQUE, A. 2005. Phanerozoic geological evolution of northern and central Africa: an overview. *Journal of African Earth Sciences* **43**, 83–143.

GUIRAUD, R., DOUMNANG MBAIGANE, J.-C., CARRETIER, S. & DOMINGUEZ, S. 2000. Evidence for a 6000 km length NW-SE-striking lineament in northern Africa: the Tibesti lineament. *Journal of the Geological Society, London* **157**, 897–900.

GUIRAUD, R., ISSAWI, B. & BELLION, Y. 1985. Les lineaments guineo-nubiens: un trait structural majeur l'echelle de la plaque africaine. *Comptes Rendus Hebdomadaires des Seances de l'Academie des Sciences* **300**, 17–20.

HAWKESWORTH, C. & SCHERSTEN, A. 2007. Mantle plumes and geochemistry. *Chemical Geology* **241**, 319–31.

HOHNDORF, A., MEINHOLD, K.-D. & VAIL, J. R. 1994. Geochronology of anorogenic igneous complexes in the

Sudan: isotopic investigations in North Kordofan, the Nubian Desert and the Red Sea Hills. *Journal of African Earth Sciences* **19**, 3–15.

ISSEINI, M., ANDRE-MAYER, A.-S., VANDERHAEGHE, O., BARBEY, P. & DELOULE, E. 2012. A-type granites form the Pan-African orogenic belt in south-western Chad constrained using geochemistry, Sr-Nd isotopes and U-Pb geochronology. *Lithos* **153**, 39–52.

KRONER, A. 1980. Pan African crustal evolution. *Episodes* **3**, 3–8.

KING, S. D. 2005. North Atlantic topographic and geoid anomalies: the results of a narrow ocean basin and cratonic roots? In *Plates, Plumes, and Paradigms* (eds G. R. Foulger, J. H. Natland, D. C. Presnall, & D. L. Anderson), pp. 653–64. Geological Society of America, Special Paper no. 388.

KING, S. D. & ANDERSON, D. L. 1998. Edge-driven convection. *Earth and Planetary Science Letters* **160**, 289–96.

KING, S. D. & ANDERSON, D. L. 1995. An alternative mechanism of flood basalt formation. *Earth and Planetary Science Letters* **136**, 269–79.

LAY, C. & REICHELT, R. 1971. Sur l'age et la significance des intrusions de dolerites tholeitique dans le basin de Taoudenni (Afrique Occidentale). *Comptes Rendus de l'Academe des Sciences* **272**, 374–6.

LIEGEOIS, J.-P., ABDELSALAM, M. G., ENNIH, N. & OUSBADI, A. 2013. Metacraton: nature, genesis and behavior. *Gondwana Research* **23**, 220–37.

LIEGEOIS, J.-P., BERTRAND, H., BLACK, R., CABY, R. & FABRE, J. 1983, Permian alkaline undersaturated and carbonatite province, and rifting along the West African craton. *Nature* **305**, 42–3.

LIEGEOIS, J.-P., SAUVAGE, J. F. & BLACK, R. 1991. The Permo-Jurassic alkaline province of Tadhak, Mali: geology, geochronology and tectonic significance. *Lithos* **27**, 95–105.

MASSA, D. & DELORT, T. 1984. Evolution du basin de Syrte (Libye) du Cambrien au Cretace basal. *Bulletin de la Societe geologique de France* **XXVI**, 1087–96.

ODIN, G. S. et al. (35 collaborators). 1982. Interlaboratory standards for dating purposes. In *Numerical Dating in Stratigraphy* (ed. G. S. Odin), pp. 123–49. Chichester: Wiley and Sons.

PEATE, D. 1997. The Parana-Etendeka province. In *Large Igneous Provinces: Continental, Oceanic, and Planetary Flood Volcanism* (eds J. J. Mahoney & M. E. Coffin), pp. 217–45. American Geophysical Union, Geophysical Monograph Series vol. 100. Washington, DC, USA.

PENAYE, J., KRONER, A., TOTEU, S. F., VAN SCHMUS, W. R. & DOUMNANG, J.-C. 2006. Evolution of the Mayo Kebbi region as reveal by zircon dating: an early (ca. 740 Ma) Pan-African magmatic arc in south-western Chad. *Journal of African Earth Sciences* **44**, 530–42.

RAHAMAN, M. A., VAN BREEMEN, O., BOWDEN, P. & BENNETT, J. N. 1984. Age migrations of anorogenic ring complexes in northern Nigeria. *Journal of Geology* **92**, 173–84.

RENNE, P. R., MUNDIL, R., BALCO, G., MIN, K. & LUDWIG, K. R. 2010. Joint determination of 40K decay constants and $^{40}Ar*/^{40}K$ for the Fish Canyon sanidine standard, and improved accuracy for $^{40}Ar/^{39}Ar$ geochronology. *Geochimica et Cosmochimica Acta* **74**, 5349–67.

ROGERS, J.J., UNRUG, R. & SULTAN, M. 1995. Tectonic assembly of Gondwana. *Journal of Geodynamics* **19**, 1–34.

SCHLUTER, T. 2008. *Geological Atlas of Africa*. Berlin: Springer-Verlag, 307 pp.

SHELLNUTT, J. G., WANG, K.-L., ZELLMER, G. F., IIZUKA, Y., JAHN, B.-M., PANG, K.-W., QI, L. & ZHOU, M.-F. 2011. Three Fe-Ti oxide ore-bearing gabbro-granitoid complexes in the Panxi region of the Permian Emeishan large igneous province, SW China. *American Journal of Science* **311**, 773–812.

SUN, S.-S. & MCDONOUGH, W. F. 1989. Chemical and isotopic systematics of oceanic basalts: implications for mantle composition and processes. In *Magmatism in the Ocean Basins* (eds A. D. Saunders & M. J. Norry), pp 313–435. Geological Society of London, Special Publication no. 42.

TOTEU, S. F., PENAYE, J. & DJOMANI, Y. P. 2004. Geodynamic evolution of the Pan-African belt in central Africa with special reference to Cameroon. *Canadian Journal of Earth Sciences* **41**, 73–85.

TOTEU, S. F., PENAYE, J., DELOULE, E., VAN SCHMIS, W. R. & TCHAMEN, R. 2006. Diachronous evolution of volcano-sedimentary basins north of the Congo craton: insights from U-Pb ion microprobe dating of zircons from the Poli, Lom and Yaounde groups (Cameroon). *Journal of African Earth Sciences* **44**, 428–42.

VAIL, J. R. 1989. Ring complexes and related rocks in Africa. *Journal of African Earth Sciences* **8**, 19–40.

VEEVERS, J. J. 2003. Pan-African is pan-Gondwanaland: oblique convergence drives rotation during 650–500 Ma assembly: *Geology* **31**, 501–4.

WEIS, D., LIEGEOIS, J.-P. & BLACK, R. 1987. Tadhak alkaline ring-complex (Mali): existence of U-Pb isochrones and "Dupal" signature 270 Ma ago. *Earth and Planetary Science Letters* **82**, 316–22.

WILSON, M. & GUIRAUD, R. 1992. Magmatism and rifting in western and central Africa, from Late Jurassic to recent times. *Tectonophysics* **213**, 203–25.

WILSON, M., GUIRAUD, R., MOREAU, C. & BELLION, Y. J.-C. 1998. Late Permian to recent magmatic activity on the African-Arabian margin of Tethys. In *Petroleum Geology of North Africa* (eds D. S. MacGregor, R. T. J. Moody & D. D. Clark-Lowes), pp. 231–63. Geological Society of London, Special Publication no. 132.